Modeling the effects of aerial temperature and exposure period on intertidal mudflat profiles

Hieu M. Nguyen[1*] | Karin R. Bryan[1,2] | Zeng Zhou[3] | Conrad A. Pilditch[1]

[1]School of Science, University of Waikato, Private Bag, 3105, Hamilton, New Zealand

[2]Environmental Research Institute, University of Waikato, Private Bag, 3105, Hamilton, New Zealand

[3]Jiangsu Key Laboratory of Coast Ocean Resources Development and Environment Security, Hohai University, Nanjing 210098, China

Correspondence

Zeng Zhou, Jiangsu Key Laboratory of Coast Ocean Resources Development and Environment Security, Hohai University, Nanjing 210098, China

Email: zeng.zhou@hhu.edu.cn

Hieu M. Nguyen, School of Science, University of Waikato, Private Bag, 3105, Hamilton, New Zealand

Email: hieugeo@gmail.com

Abstract

This research demonstrates how the effect of exposure to air on intertidal flat profile development in cohesive coastal environments can be incorporated into applied numerical modelling. Semi-empirical relationships were used to include the sediment stabilizing effects of exposure on changes to the erosion threshold (τ_{cr}; $N\ m^{-2}$) and erosion rate (ER; $g\ m^{-2}\ s^{-1}$) during low tide, which also take into account the effect of air temperature, T (°C) and exposure duration, D (h). The relationships were based on fundamental forms of the theoretical relationship between water content and evaporation rate, and were fitted to empirical data. Changes were incorporated into the Delft3D model, and scenarios monitored bed level profile development over an annual time scale with different T, sediment stabilizing biofilm biomass (using *Chl-a* content as a proxy), initial bed composition (mud/sand percentage), and spring and neap tides (regulating current velocity and exposure duration). Model results indicated that the stabilizing effect of exposure will lead to a more flat-topped shape of intertidal mudflats, implying that bed level changes caused by exposure occur lower on intertidal flats compared to runs with no exposure. Higher air temperatures had a greater effect on bed level change, with the maximum accretion of up to 0.039 m (290% higher) occurring in the case of 40 °C compared with the case of no exposure effect with 0.01 m of accretion. Research findings will contribute to understanding of how intertidal flats evolve and is critical to predicting the resilience of these habitats to sea-level rise and warming temperatures.

Keywords: cohesive sediments, bed level change, numerical simulation, sediment stability, low-lying areas, Delftd3D, critical erosion threshold, erosion rate

Introduction

Understanding the evolution of coastal morphology is critical to planning how we adapt to sea-level rise (SLR). Some models suggest that low-lying areas will gain elevation to keep pace with rising sea-levels (e.g. Kirwan et al., 2016; van Maanen et al., 2013; Fagherazzi et al., 2006; Marani et al., 2007); conversely, other studies predict high sensitivity to the rate of SLR, and sediment supply and retention of sediment may not be insufficient (e.g. Fagherazzi et al., 2006; Marani et al., 2007). Consequences stretch beyond the simple loss of coastal land. Rising sea-levels can also change our exposure to ocean hazards such as waves and storm surges (and effectiveness of eco-defences), suspend new sediment from recently-inundated areas (Mi et al., 2020) and change coastal light regimes (Mangan et al., 2020), affecting primary productivity and ecosystem structure and function (e.g. Pratt et al., 2014).

Many studies have modelled the evolution of low-lying coastal land, both in mangrove-dominated tropical and subtropical areas, and in more temperate salt marshes. For example, Mariotti and Fagherazzi (2010) presented a numerical model for the coupled long-term evolution of salt marshes and intertidal flats, confirming that expansion or erosion of salt marshes is a function of SLR rate in combination with parameters such as sediment supply. A low rate of SLR induced marsh expansion while a high rate resulted in drowning of salt marshes. Even in cases where land keeps pace with sea-level rise, the size, shape and location of the intertidal areas will likely change (van Maanen et al., 2013).

One of the primary controls on how the coastal landscape functions (in terms of both ecological and socio-economic values) is the shape of the intertidal profile. Intertidal profiles can be concave or convex depending on such factors as relative intensity of wave and tidal forcing, sediment supply and grain size, and the local elevation of the flat relative to the mean sea level (Bearman et al., 2010). Tidal currents enhance convexity whereas waves favour concavity (Friedrichs et al., 1996; Pritchard and Hogg, 2003; Zhou et al., 2015). Sandier tidal flats, in turn, tend to be associated with wave-dominated areas, and muddier flats are more common in tide-dominated areas (Yang et al., 2008; Zhou et al., 2015). Erosional flats tend to be more concave upward, meanwhile accretionary tidal flats are observed to become more convex upward (Dyer, 1998; Kirby, 2000; Le Hir et al., 2000; Mehta, 2002; Van Rijn, 1998), an effect which becomes more pronounced with increased tidal range (Friedrichs, 2011; Kirby, 2000).

Recent modelling exercises have focused on reproducing these subtle variations in the profile of intertidal flats. For example, an elegant analytical solution to predict equilibrium profiles of tidal flats for both wave and tide dominated environments was derived by assuming that equilibrium occurred when the spatial distribution of

maximum bottom shear stress reached uniformity (Friedrichs et al., 1996; Zhou et al., 2016). Similar numerical models were developed using mass conservation and momentum balance to simulate mudflat profile changes (Roberts et al., 2000). Zhou et al. (2015) extended this work and developed a numerical model to investigate morphodynamics of intertidal flats, in particular examining the effect of sediment parametrization (i.e. the effect of initial bed sediment composition and sediment sources on the shape of intertidal flats). A larger mud concentration at the sea boundary promotes seaward advance and more convex-up intertidal flats (Liu et al., 2011; Pritchard et al., 2002; Pritchard and Hogg, 2003; Roberts et al., 2000; Zhou et al., 2015). A tidal flat with initially a larger percentage of mud tends to make the profile more convex up (Friedrichs, 2011; Kirby, 2000; Zhou et al., 2015), associated with the reduced erodibility of muddy sediment.

One of the effects that has not been well considered yet in profile models is the effect of atmospheric exposure on the properties of cohesive intertidal sediments. Recent work has shown that exposure to air during low tide can have pronounced effect on the erodibility of cohesive sediments (Fagherazzi et al., 2017; Nguyen et al., 2019; Nguyen et al., 2020), even more than grain size variations and bio-stabilisation by microphytobenthos (biofilms). Depending on the atmospheric conditions during exposure and the duration, evaporation decreases the water content of sediments, which in turn increases erosion resistance (by increasing erosion threshold and decreasing erosion rate). These effects are in addition to the stabilizing effects of biofilm growth on sediment surface. Both evaporation and biofilms stabilise the sediment by strengthening bonds between particles and increasing the drag force required on the bed surface to cause erosion (Fagherazzi et al., 2017; Paterson, 1989; Tolhurst et al., 2006a; Underwood and Paterson, 2003; Widdows et al., 1998), with the strengthening effect remaining in subsequent flooding cycles (Fagherazzi et al., 2017; Nguyen et al., 2020). Laboratory measurements show an interaction between evaporation and biofilm growth that ultimately controls sediment erosion properties (Nguyen et al., 2020). For instance, after 10 days exposure critical erosion stress (T_{cr}) increased by 1.7 (low biofilm biomass) to 4.4 (high biofilm biomass) times and the erosion rate (*ER*) decreased by 11.6 to 21.5 times compared with compared with 6 h of exposure. Conversely, exposure to rain during low tide destabilises sediments (Pilditch et al. 2008; Tolhurst et al. 2006b), by reducing bonding between particles.

This study aims to incorporate recent understanding on the changes to sediment properties that occur during short periods of exposure into numerical coastal profile modelling. Here, we hypothesize that the change in erodibility of sediments caused by exposure (including exposure temperature (*T* °C) and duration (*D* h)) as well as *Chl-a* content (a proxy of biofilm biomass) can change the way in which coastal profiles evolve. We used Delft3D to develop the numerical model, so that innovations added to the model can be made available through their open-source community. In addition, the effects of exposure temperature, *Chl-a* content, initial sediment bed composition (percentage of mud and sand) and spring and neap tidal cycles (effects current velocity and exposure period) on intertidal flat profile development were also investigated using the modifications to the bed transport sub-routines of Delft3D. The overarching aim of our work is to show how understanding exposure

effects in sediment transport modelling could be critical to predicting the resilience of intertidal zones into the future, when sea-level rise may exacerbate erosion in low-lying areas.

Methods

- **Modelling of erosion properties**

The relationship between air temperature - *T* and exposure duration - *D* on the critical bed shear stress (T_{cr}, *N* m^{-2}) and erosion rate *ER* (*g* m^{-2} s^{-1}) were expressed using semi-empirical models fitted to the data collected in Nguyen et al., (2019) (Exp. 1) and Nguyen et al., (2020) (Exp.2). The form of these models was based on the theoretical relationship between water content and evaporation rate, which depends on *T* and *D* (Nguyen et al., 2020). However, the coefficients were fitted empirically from experimental data because they depend on a number of complex and unknown effects such as the role of organic content in regulating moisture, the rate of vertical water movement through the sediment surface and the role of biofilms in binding the surface particles (bio-stabilization). T_{cr} and *ER* were determined using a core based erosion device (EROMES) on sediment collected from a cohesive intertidal site at different times of the year and subjecting them to differing exposure periods (see Nguyen et al., 2019, 2020 for details).

In Exp.1, temperature was varied while holding the exposure duration constant at 6 h using treatments of sediments with high and low *Chl-a*, while in Exp.2 exposure duration was varied in two trials to represent typical summer and winter conditions. In Exp. 1, exposure temperature was controlled at 0, 8, 25 and 40°C to examine its effect on sediment erodibility. Exp. 2 exposed sediment cores to natural outdoor ambient conditions for 6 h, 1, 4 and 10 d with air temperature being logged every minute. Sediments used in both experiments were collected from intertidal mudflats in the Firth of Thames, New Zealand between 2017 and 2019 and collection times represented both winter and summer conditions. Overall, *Chl-a* content of winter samples were significantly lower than that of summer samples, while particle median grain size did not differ significantly between seasons (Table 1). Note that these experiments were not specifically designed to parameterize this model and so a full range of combinations of *Chl-a*, temperature and exposure is not available.

Table 1 In situ sediment properties at the time cores were collected for use in laboratory experiments (data summarized from Nguyen et al., (2019) and Nguyen et al., (2020)).

Properties	Dec 2017	Mar 2018	Oct 2018	Jan 2019	Feb 2019
Wet bulk density (g cm^{-3})	-	-	1.36 ± 0.08	1.44 ± 0.05	1.43 ± 0.07
Dry bulk density (g cm^{-3})	-	-	0.32 ± 0.03	0.34 ± 0.06	0.33 ± 0.04
Median grain size (D_{50}, µm)	6.37 ± 1.05	8.90 ± 0.90	6.34 ± 1.72	6.94 ± 1.59	6.14 ± 0.85
Clay content (%)	37.8 ± 4.1	26.3 ± 2.8	37.6 ± 6.2	34.1 ± 5.2	34.8 ± 4.0
Silt content (%)	55.3 ± 5.3	63.4 ± 3.8	55.8 ± 4.1	62.8 ± 5.1	61.2 ± 5.0
Sand content (%)	6.9 ± 2.8	10.3 ± 3.1	6.6 + 3.98	3.1 ± 0.9	4.0 ± 1.0
Chlorophyll-a (*Chl-a*, µg g^{-1})	9.2 ± 2.7	21.6 ± 5.8	10.8 ± 1.9	78.0 ± 13.0	65.1 ± 6.2
Organic content (*OC*, %)	9.8 ± 0.3	10.1 ± 3.2	10.3 ± 0.6	12.6 ± 0.5	13.1 ± 0.4

- *Data represent the mean ± 1 standard deviation (n=20*)

While a linear model best fitted the relationship between T_{cr} and T and D (Figure 1A and 1C), an exponential model best described the relationship between ER and these two factors (Figure 1B and 1D). Both models needed to include an interaction term, so that at the moment of exposure, the T_{cr} and ER values were equal to the submerged values, regardless of exposure temperature. Nguyen et al. (2019, 2020) showed that the change in biofilm biomass on the intertidal flat was seasonal, with a higher *Chl-a* biomass in summer and lower in winter (Table 1). Data were therefore separated into high and low *Chl-a* content treatments to examine the effect of biofilm biomass on sediment erosion potential. In addition, pooled data from both the high and low *Chl-a* content were used to inform a general model. Our best fitted model resulted in the following equations for T_{cr} and ER:

$$ER = ER_{inn} \times e^{(a_1 T + a_2)D} \quad (1)$$

$$\tau_{cr} = \tau_{inn} + (b_1 T + b_2)D \quad (2)$$

Where τ_{inn} and ER_{inn} are erosion threshold and erosion rate of sediment when inundated, respectively and the a_1, a_2, b_1, b_2 are coefficients which were evaluated separately for high and low *Chl-a* content cases and the pooled data (see Table 2 for coefficient values).

Table 2 Coefficients model for erosion rate (Eq. 1: $ER = ER_{inn} \times e^{(a_1 T + a_2)D}$) and erosion threshold (Eq.2: $\tau_{cr} = \tau_{inn} + (b_1 T + b_2)D$) of sediment.

Chl-a cases	a_1	a_2	r^2	*F*	b_1	b_2	r^2	*F*
Pooled data	-0.0034	0.0173	0.23	2.2	0.0029	-0.02	0.57	8.5
Low *Chl-a* data	-0.0072	0.0451	0.92	31.0	0.0017	0.0101	0.81	10.8
High *Chl-a* data	-0.0077	0.0716	0.98	132.4	0.0032	-0.023	0.98	181.0

- *Pooled: mean Chl-a is 31.8, µg g^{-1}*
- *Low (Dec 2017&Mar 2918&Oct 2018): mean Chl-a is 15.0, µg g^{-1},*
- *High (Jan 2019&Feb 2019): mean Chl-a is 48.6, µg g^{-1}*

The strengthening effect of exposure on sediment stability is believed to remain over subsequent flooding cycles (Fagherazzi et al., 2017). Nguyen et al., (2020) demonstrated this by conducting re-submersion experiments on intertidal cohesive sediments after exposure periods of 1, 4 and 10 d. Their results showed that erosion resistance of exposed sediments showed no significance changes after one and two re-submersion events (each lasting for 4 h). However, to retain the potential that sediments recover to initial conditions (when re-inundated) after much shorter exposure times than covered in our experiments (for example, a single tidal cycle), we added recovery coefficients for T_{cr} and *ER* into the models, which allow sediment erosion properties to gradually return to submerged conditions when immersed. The more the erosion properties changed during exposure (e.g. higher *T* and longer *D*), the longer the recovery period (see below for details).

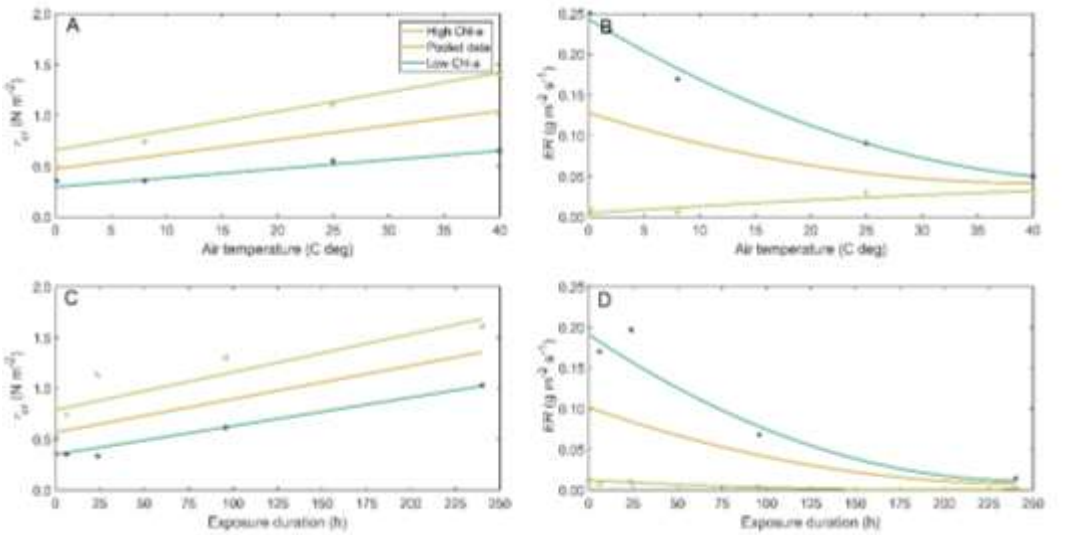

Figure 1 Empirical models for A & C) erosion threshold T_{cr} (N m^{-2}) and B & D) erosion rate *ER* (g m^{-2} s^{-1}), fitted to the experimental results of Nguyen et al. (2019, 2020).

- **Model setup**

Following Roberts et al. (2000), the starting bed profile was linearly sloped from an elevation of 6 m (below Mean Sea Level, MSL) to 4 m above MSL over a distance of 10 km (i.e., slope is 0.1%, Figure 2A. This is a similar slope to the field site in Nguyen et al. (2019, 2020). The bed was covered with a 5 m sediment layer which was composed of sand and mud. The offshore tidal boundary was forced by the superposition of M_2 and S_2 constituents to simulate the spring-neap cycle. The spring tidal range was set as 3 m (the tidal range at the field site). The erosion threshold and erosion rate when the profile was inundated were set to 0.05 $N\ m^{-2}$ and 0.05 $g\ m^{-2}\ s^{-1}$ respectively, the values that were measured from erosion experiments on cores which were retained in a submerged state (sediment samples were submerged for 6 h prior to tests for erosion properties) from Nguyen et al. (2019, 2020).

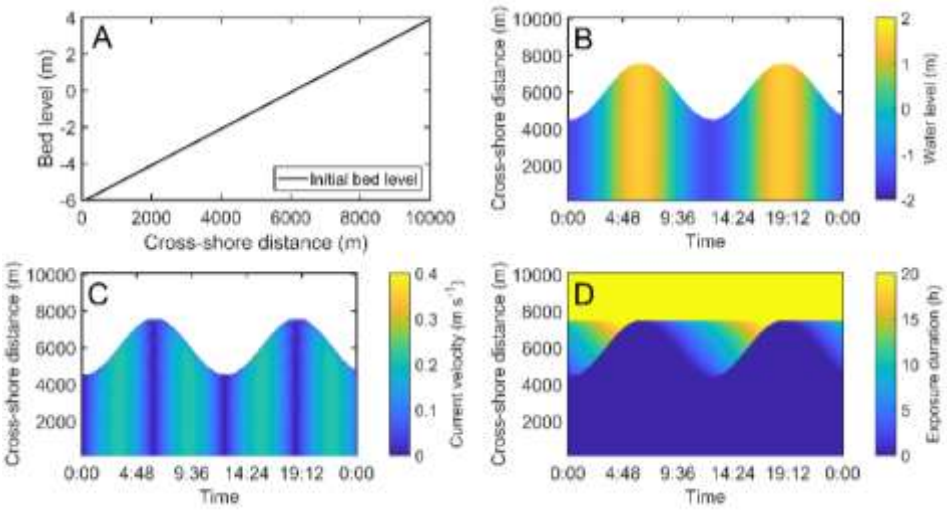

Figure 2 An example of model results (20 °C air temperature) showing A) initial bed level B) water level, C) current velocity and D) exposure duration.

Model scenarios were designed to explore the role of air temperature, spring and neap tides, biofilms, and bed sediment texture (percentage of sand/mud in the bed composition) on profile evolution (summarized in Table 3). Three model runs of 10, 20 and 40 °C were chosen to investigate the effect of air temperature, which covers a wide range of temperature and the extremes that occur at our field site. In other model runs that examine the influence of spring and neap tides, biofilms and sediment composition, the air temperature was set at 20 °C. As a first attempt to understand the role of exposure on profile development, models were run for one year to simulate the initial influence on intertidal flats. Further work will explore the role of seasonality and precipitation on profile development.

Table 3 Parametrizations for the model setup

T (°C)	τ_{inn} (N m^{-2})	ER_{inn} (g m^{-2} s^{-1})	*Chl-a* content cases	Sand / Mud (%)	Tide constituents (m)
10	0.05	0.05	Pooled data	Mud only	M_2=1.5 S_2=0
20	0.05	0.05	Pooled data	Mud only	M_2=1.5 S_2=0
40	0.05	0.05	Pooled data	Mud only	M_2=1.5 S_2=0
20	0.05	0.05	Pooled data	Mud only	M_2=1.5 S_2=0
20	0.05	0.05	Pooled data	Mud only	M_2=1.5 S_2=0.45*
20	0.05	0.05	high Chl-a	Mud only	M_2=1.5 S_2=0
20	0.05	0.05	low Chl-a	Mud only	M_2=1.5 S_2=0
20	0.05	0.05	Pooled data	50/50	M_2=1.5 S_2=0
20	0.05	0.05	Pooled data	30/70	M_2=1.5 S_2=0
20	0.05	0.05	Pooled data	70/30	M_2=1.5 S_2=0

- *M_2 and S_2 are the principal lunar and solar semi-diurnal constituents, respectively.*
- *The "no exposure effect" case is set up with constant values of erosion threshold and erosion rate at 0.05 N m^{-2} and 0.05 g m^{-2} s^{-1}, bed composition of 100 % mud, and M_2 = 1.5 m, S_2 = 0 m.*

**Spring-neap tide case.*

- **Formulae controlling sediment dynamics**

In Delft3D, sand and mud fractions are considered individually. Therefore, physical process such as erosion and deposition are treated separately for each fraction. Sediment transport of cohesive fractions – mud is modeled using an advection equation

$$Q_{mud,e} - Q_{mud,d} = \frac{\partial (Ch)}{\partial t} + \frac{\partial (uCh)}{\partial x} \quad (3)$$

where $Q_{mud,e}$ and $Q_{mud,d}$ are erosion and deposition fluxes, respectively. C is depth averaged concentration (kg m^{-3}), h is water depth (m), u is depth averaged flow velocity (m s^{-1}), t is time (s), x is direction (m). These fluxes were modelled using the widely adopted Partheniades–Krone equations (Partheniades, 1965)

$$Q_{mud,e} = \begin{cases} ER\left(\frac{\tau_{max}}{\tau_{cr}} - 1\right) & if\ \tau_{max} > \tau_{cr,e} \\ 0 & if\ \tau_{max} \leq \tau_{cr,e} \end{cases} \quad (4)$$

$$Q_{mud,d} = \begin{cases} W_s C\left(1 - \frac{\tau_{max}}{\tau_{cr,d}}\right) & if\ \tau_{max} < \tau_{cr,d} \\ 0 & if\ \tau_{max} \geq \tau_{cr,d} \end{cases} \quad (5)$$

where ER is the erosion rate (g m^{-2} s^{-1}, described as the erosion parameter - M_e in Partheniades (1965)), τ_{cr} and $\tau_{cr,d}$ are the bed shear stress for the erosion threshold and deposition of the mud component, respectively (N m^{-2}). τ_{max} is the maximum bed shear stress (N m^{-2}) and W_s is the settling velocity (m s^{-1}). $\tau_{cr,d}$ is set at very large value of 1000 N m^{-2} as default (Winterwerp, 2007), which means that sediments always deposit when conditions are below the erosion threshold.

In traditional Delft3D modeling studies of sediment dynamics and bed level change, ER and τ_{cr} (in Equation 4) are typically set as constants and do not change with exposure. In this research, we have extended Equation 4 by embedding the formulations of ER and τ_{cr} described by Equation 1 and 2 into Delft3D. The air temperature to which the intertidal sediments are exposed was set as a constant value along with the empirical coefficients in Table 2. The duration of exposure is introduced as a new model variable, which depends on the bed level on the tidal flat, and is determined by whether the bed level is above or below the water level at each hydrodynamic time step. Also included is a new variable which determines the time over which the sediment returns to pre-exposure conditions after re-inundation. This was assumed to be a linear function (given that we have no experimental data on which to base a relationship), so that τ_{cr} decreases and ER increases with time (both rates set in the input file).

$$ER(t) = ER_{inn} + Rev_{ER} * t, \quad (6)$$

$$\tau_{cr}(t) = \tau_{inn} - Rev_{Tau} * t, \quad (7)$$

where $ER(t)$ (g m^{-2} s^{-1}) and $\tau_{cr}(t)$ are erosion rate and erosion threshold of submerged sediments at a given time t (minute), Rev_{ER} and Rev_{Tau} are arbitrarily-set recovery coefficients of erosion rate and erosion threshold, respectively. The recovery coefficients are set at a constant value for each model run and each exposure air temperature.

Figure 2B, 2C and 2D present an example of a model setup in which the exposure duration at different levels on the intertidal flat was computed in the Delft3D sediment transport modules using the water level and bed elevation, and the current velocity during flood and ebb tides associated with each water level were calculated in the basic Delft3D hydrodynamic drivers. Two sets of runs were completed for each scenario: one with low time resolution over a whole year to track morphological change, and a shorter run at a higher time resolution to create detailed figures of the suspended sediment flux and currents for interpretation.

Results

- **Effect of air temperature on bed level change**

In order to examine the effect of T on τ_{cr} and ER (Figure 3) and their ultimate control on bed level, models were run with T set to 10, 20 and 40 °C while tidal ranges (tide constituents of M_2 = 1.5 m and S_2 = 0 m) were held constant. In model runs with no exposure effect (i.e. in which the exposure effects on sediment stability during low tide was neglected), τ_{cr} and ER were unchanged during tidal cycles and were equal to inundated values (Figure 3A and 3B). In this case, there is a strong increase in suspended sediment concentration as the flooding tide moves over the intertidal region, which is not matched by a peak in ebbing suspended sediment concentration (Figure 3C). In comparison, when the effect of exposure is taken into account, model results indicated that intertidal sediments were stabilized during exposure with higher values of τ_{cr} and lower values of ER with the rate of increase/decrease dependent on T. Maximum values of τ_{cr} increased from 0.05 to 0.15, 0.5, 1.6 $N\ m^{-2}$, while maximum values of ER decreased from 0.05 to 0.035, 0.02, 0.01 $g\ m^{-2}\ s^{-1}$ in accordance with T of 10, 20, 40 °C. In these scenarios, the ebb and flood tide suspended sediment concentrations are more similar in magnitude; when the bed is more stable, less sediment is eroded during the incoming tide. The flooding currents only start eroding sediments in the intertidal after the stabilization effect has worn off. As we employed a recovery factor for the values of τ_{cr} and ER, the recovery of these values in the subsequence flooding cycles will depend on how much change the values gained during the exposure periods (Figure 3D, 4.3E, 4.3G, 4.3H, 4.3J and 4.3K). Consequently, τ_{cr} and ER took longest time to return to inundated values for the case of 40 °C (Figure 3K-in which case the erosion threshold never returns to the submerged value), whereas these values recovered more quickly for the cases of 10°C and 20°C (returning to the submerged values before the ebbing tide drains from the intertidal region). The model simulates the amount of water lost by evaporation during exposure and the higher temperature caused more water to evaporate.

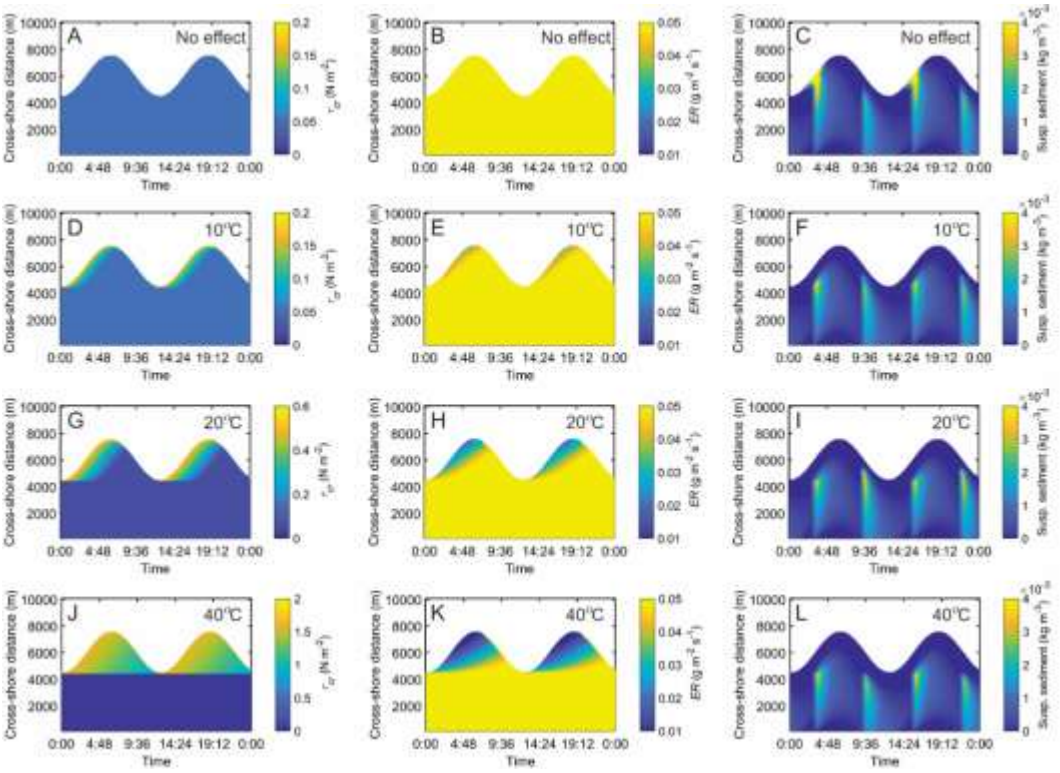

253

254 Figure 3 Effect of air temperature on T_{cr} (A, D, G, J), ER (B, E, H, K) and suspended sediment concentration (C, F,
255 I, L). Note figures show variations over two tidal cycles and the colour scale has different ranges for the left
256 column panels.

257 In general, net erosion occurred in the sub-tidal zone area while accretion occurred in the intertidal zone in all
258 cases (Figure 4A). With no exposure effect, the change in bed level was evenly-distributed across the intertidal
259 zone, except for minor erosion within the zone from 5100 m to 5500 m in the cross-shore (Figure 4A). The
260 positive change of bed level was more evident within the upper part of the intertidal (5500 m-7000 m) and
261 erosion mostly occurred in sub-tidal zone (Figure 4A). The pattern of bed level change could be explained by the
262 cross-shore distribution of sediment flux (Figure 4B); the flood peak in the sediment flux occurs at a higher tidal
263 stage than the ebbing flux, causing a flux shoreward of sediment in the intertidal area. In fact, there is only a
264 flooding sediment flux on the upper intertidal (the ebb-flux is non-existent), and the flood tide sediment flux
265 always surpasses that of the ebb tide in the intertidal. In the no exposure effect scenario, the imbalance between
266 flood and ebb sediment flux would eventually cause the profile to flatten in the intertidal region (a convex profile
267 development).

268 When the effect of air temperature is considered in the model, accretion of sediment on intertidal flat tended
269 to focus on the lower intertidal, in comparison to the 'no effect case' (Figure 4A). On the lower flat, a bed level
270 increase of from 0.02 (T = 10 °C) to 0.039 m (T = 40 °C) occurred compared to less than 0.01 m for the no exposure
271 effect case. In contrast, on the higher intertidal, sediment accretion of 0.022 m occurred for no effect case
272 compared with less than 0.01 m for cases when the temperature exposure effect was included. Higher T resulted

in more sediment accumulation on the intertidal flat as a consequence of increased net sediment erosion in the sub-tidal zone. The currents are approximately the same in all the scenarios, so the difference in net sub-tidal erosion is likely because the sediment is more effectively trapped in the intertidal zone and not available to be transported seaward by the sub-tidal ebb currents (Figure 4B, green line at 4000m). (Whereas in the no-exposure effect case, sub-tidal erosion by the flooding tide is partially compensated by accretion during the ebbing tide). Within the intertidal, there was a transition from the upper to the lower intertidal (seaward) of the accumulation zone between the 10 °C case and the cases with higher air temperature (20 °C and 40 °C), which would cause the intertidal profile to become flatter and the lower edge of the intertidal to become steeper. At higher elevations, the difference in sediment flux between the ebb-tide and flood-tide becomes more evident, for example from 5500 m shoreward there were only flood-directional sediment fluxes. The higher elevations on the intertidal flats are progressively exposed for increasing times, which means that the sediments there become increasingly more stable with temperature, and there is no source of sediment provided to the ebbing currents to carry seaward— therefore as temperature increases, more and more sediment accumulates on the lower intertidal. In summary, the larger the stabilizing effect (e.g. 40 °C), the larger the effect on the bed level.

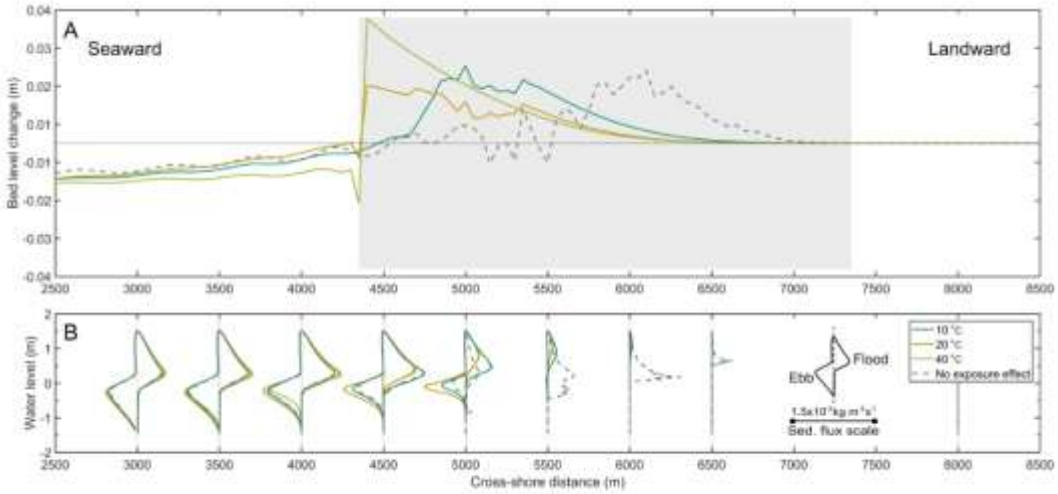

Figure 4 Effect of air temperature on bed level changes over one year, modelled using tide constituents M_2 = 1.5, S_2 = 0 (shaded area represents the inter-tidal area), using the pooled data *Chl-a* model, bed sediment composition mud only, ER_{inn} = 0.05 g m^{-2} s^{-1}, and τ_{inn} = 0.05 N m^{-2}. The sediment flux scale is the same for each vertical sediment flux profile plot (scale bar plotted at the right side).

- **Effect of biofilms on bed level change**

In order to examine the effect of biofilm stabilization, models were set up for low and high *Chl-a* content with the same temperature, bed composition and tidal conditions. Note that the low and high *Chl-a* runs represent different erosion values measured in experiments taken in winter and summer which were accompanied by

changes to *Chl-a*; however experiments were not set up to test *Chl-a* effects on erosion, and so we cannot conclusively prove that observed changes to erosion conditions were caused by *Chl-a*. Instead, these runs should be consider as a demonstration of the sensitivity of bed-level changes to seasonal differences in conditions. Parametrizations used in the model are presented in Table 3. We assume that the difference in *Chl-a* only effect the intertidal regions, the subtidal erosion characteristics remain constant between all runs (Table 3). In fact, in the low *Chl-a,* the intertidal conditions are less stable than the subtidal. Bed level changes were substantially different between low and high *Chl-a* content cases (Figure 5A). For both the pooled data and the high *Chl-a* model runs, sediment started accumulating from 4350 m (at the seaward extent of the intertidal) then accumulation gradually decreased over the intertidal flat, with maximum changes of 0.015 m and 0.005 m for the former and the latter, respectively. The pattern of bed level change for the low *Chl-a* cases was different to the others in that the accumulation had two maxima, one on the lower flat (4350 – 4700 m, maximum of 0.012 m) and one on the upper flat (5600 – 7000 m, maximum of 0.018 m), separated by an eroded zone (4700 – 5600 m, minimum of 0.015 m). The low *Chl-a* case had greater landward sediment flux relative to seaward sediment flux, which caused the significant change of the bed level (Figure 5B). The very different patterns at low *Chl-a* are likely due to intertidal conditions being less stable than subtidal. In general, just as with the high-temperature runs, when stabilization increases (high *Chl-a*), the supply of sediment from the intertidal regions is suppressed, meaning a reduction of the sediment scoured seaward by the ebbing current, and landward by the flooding current.

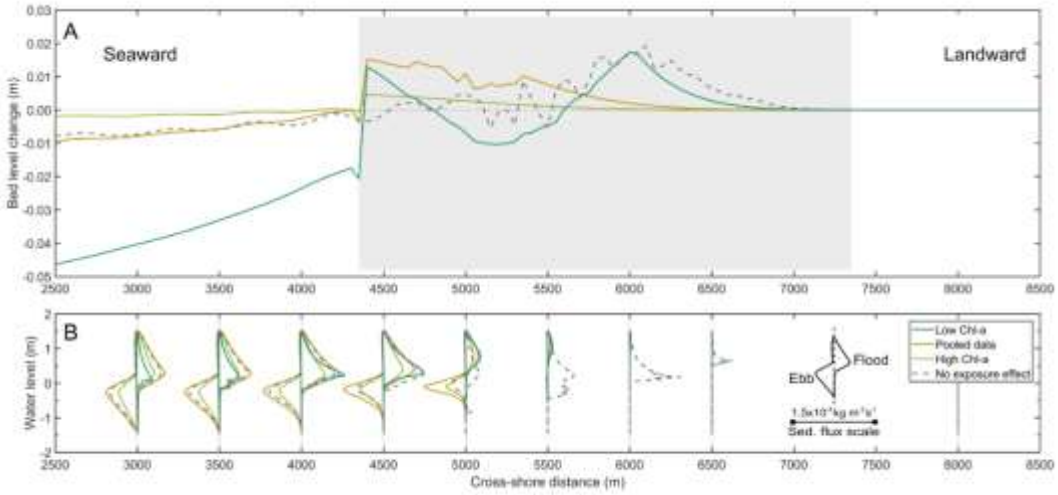

Figure 5 Effect of biofilm growth on bed level changes over one year, tidal constituents M_2 = 1.5, S_2 = 0 (shaded area represents the intertidal area), modelled with an air temperature 20 °C, bed sediment composition = mud only, ER_{inn} = 0.05 g m^{-2} s^{-1}, T_{inn} = 0.05 N m^{-2}. The sediment flux scale is the same for each vertical sediment flux profile plot (scale bar plotted at the right side).

- **Effect of bed sediment composition on bed level change**

Generally, changes to bed composition caused a similar pattern in bed level changes to the effect of changes in temperature and C*hl-a*, with an increase in the sediment accumulated in the region from 4350 to 7000 m over the intertidal flat (Figure 6A). After a year, transported sediment mostly accumulated in the zone of 4350 – 4600 m (+ 0.012 to 0.018 m), reduced in the zone of 4600 – 5200 m (+ 0.002 to 0.01m) and increased again from 5200 – 5500 m (+ 0.007 to 0.015 m) before a gradual decrease to no accumulation from 5500 – 7000 m. Bed composition with higher percentage of mud showed greater net erosion in the subtidal zone, and greater net accumulation in the intertidal. This is likely mainly because a greater fraction of the bed is affected by the differences in stabilization (the stabilization effect is only applied to the mud fraction in the model, and has no effect on the sand). It would also be in part caused by the spatial distribution of stabilisation effect (as in Figure 4), were when more sediment is trapped on the intertidal, the tide ebbing off the intertidal is deprived of sediment, and so causing a decrease of accumulation in the subtidal. Greater sediment fluxes explained the higher level of bed level change for the cases with higher percent of mud fraction (Figure 6B). For example, 100 % mud always showed the greatest sediment fluxes while with 30 % mud/70 % sand had the lowest sediment fluxes over the cross-shore section (Figure 6B).

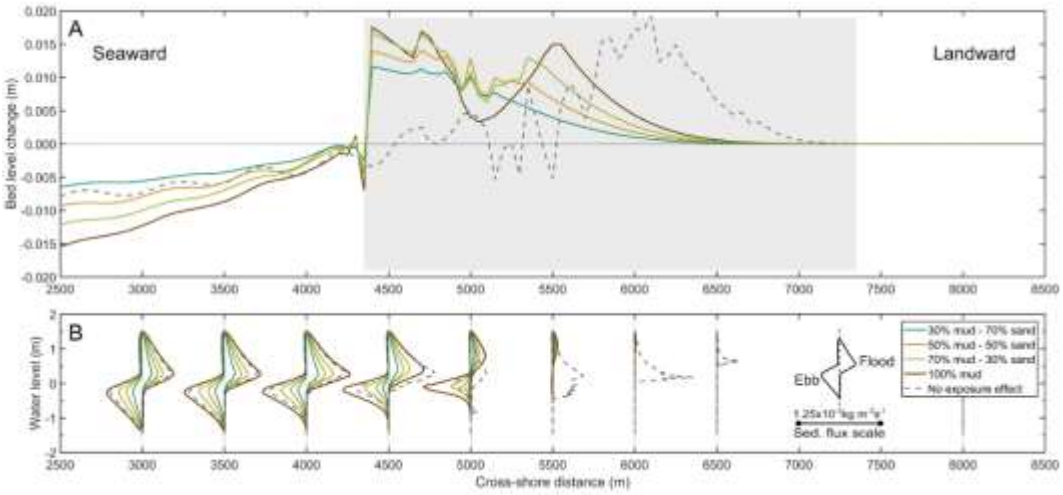

Figure 6 Effect of bed composition on bed level changes over one year, tidal constituents $M_2 = 1.5$, $S_2 = 0$ (shaded area represents the inter tidal area), air temperature 20 °C, pooled data *Chl-a* model, $ER_{inn} = 0.05\ g\ m^{-2}\ s^{-1}$, $T_{inn} = 0.05\ N\ m^{-2}$. Note that the exposure effect applied to the mud fraction only. The sediment flux scale is the same for each vertical sediment flux profile plot (scale bar plotted at the right side).

- **Effect of spring – neap tide on bed level change**

To examine the effect of changes in the tidal range in combination with the exposure effect on bed level change, a model that included spring-neap variations (with a wider tidal range - M_2 = 1.5 m, S_2 = 0.45 m) and a model with normal tidal range (M_2 = 1.5 m, S_2 = 0 m) were set up at the same temperature (20 °C; Figure 7). This meant that areas on the high intertidal could remain exposed for up to 14 days. The results indicated that a wider (spring) tidal range led to the accumulation zone moving seaward (green line) compared to the normal tide (yellow line) and with no exposure effect (black dashed line). The spring-neap tide case eroded more sediment in the sub-tidal zone seaward of 3900 m. For this case, bed level increased by 0.02 m in the zone of 3900 – 4000 m then decreased over the higher parts of the intertidal flat from 4000 – 7000 m. With a normal tide, sediment eroded in sub-tidal zone, accumulated on the lower tidal flat of up to 0.015 m then gradually decreased to 7000 m on the flat. Sediment fluxes in the spring – neap tide case always surpassed the normal tide case both with and without the exposure effect (associated with the stronger tidal currents occurring with spring tides); the asymmetry was also more flood-dominant in the spring-tide case, which resulted in wider range of bed level changes.

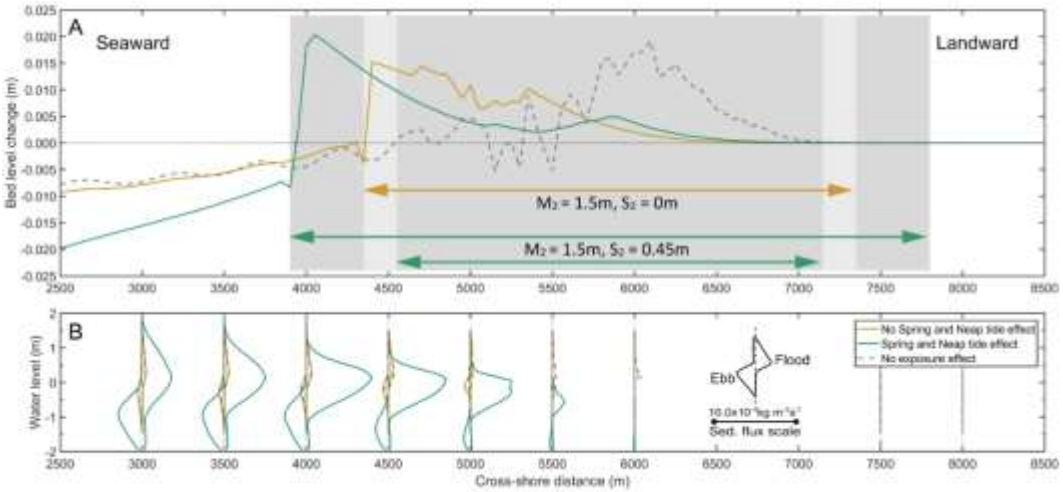

Figure 7 Effect of tide level on bed level changes over one year, air temperature 20 °C, pooled data *Chl-a* model, ER_{inn} = 0.05 g m^{-2} s^{-1}, T_{inn} = 0.05 N m^{-2}. Shaded areas represent inter tidal areas (green arrows represent spring and neap tides, golden arrow represents the intertidal tidal area for the case of no spring and neap tide effect). The sediment flux scale is the same for each vertical sediment flux profile plot (scale bar plotted at the right side).

Discussion

This paper sought to model differences that exposure of sediment to evaporation at low tide could potentially have on intertidal mudflat development, with the effect of *Chl-a* content, bed composition and tidal ranges being included in models. Areal exposure causes the surface sediment to loose moisture and the particles to bind more effectively together, increasing the critical erosion threshold and reducing the erosion rate. Both these parameters are a fundamental control to how sediment is eroded and accreted in cohesive environments. Our modelling results indicated that adding in the effect of exposure generally causes more accretion on the lower intertidal flats at sites with tidal currents that were sufficient to mobilize sediment. Consequently, the tendency to accrete means that convex tidal flats would be created in all cases if the models were run over a much longer timescale. Our results are consistent with previous studies that showed the interrelation between accumulation of sediment on intertidal flats and convexity of the profile (Dyer, 1998; Kirby, 2000; Le Hir et al., 2000; Mehta, 2002; Van Rijn, 1998). When the effect of exposure was taken into account, the formation of convex tidal flats occurred by building upward on the lower intertidal, whereas in previous studies, the convexity builds seaward as sediment accumulates on the landward fringe (Kirby, 2000).

The seaward shift of the accretion zone occurs because of the increase in stabilisation of the intertidal sediments. The sediment used to build the intertidal zone either comes from the outer boundary, or is eroded from the subtidal and lower intertidal regions. The flooding tide brings the sediment shoreward, where it settles out gradually throughout the intertidal. The following ebbing tide gathers momentum as it drains off the intertidal, resuspending the sediment on the lower intertidal, and so without any exposure effect, the sediment prefers to settle out on the higher intertidal. However, when the exposure effect is added, the suspension on the lower intertidal is dramatically reduced (compare Figure 3C and F), so there is less sediment available to supply the upper intertidal, and more retained on the lower intertidal. Retaining sediment on the intertidal also means that there is less sediment transported into the subtidal, and net erosion occurs in the subtidal. The higher the temperature, the more pronounced this effect was. The extreme scenario of 40°C caused substantially higher tidal flat accumulation (0.039 m by the end of model simulation compared with 0.022 m build-up of sediments in the no exposure effect tidal flats, corresponding to 77% higher). However, 40 °C is an extreme case, and accretion rates for exposure treatments were generally similar to no exposure treatments, but were distributed quite differently, accumulating on the lower intertidal. Sediments with higher mud content built up bed elevation more which is consistent with previous studies in which profiles with greater mud fractions causing more transport to the upper tidal flat (Zhou et al., 2015; Kirby, 2000; Friedrichs; 2011). The exposure effect was applied to the mud fraction only, therefore, the higher mud percentage the more pronounced this effect was. Interestingly, there was often a bimodal distribution of accumulation (e.g. Figure 5, low *Chl-a* and Figure 6, 100% mud). Accumulation and accretion is a product of small changes in the balance of ebbing and flooding sediment fluxes, which change across the profile. There is a point on the mid-intertidal where sediment fluxes switch locally to ebb-dominant from a pattern that is generally flood-dominant across the intertidal.

Our model results show that the effect of increasing intertidal stabilization is likely to create a more convex profile (or a more flat-topped intertidal profile). Although such profiles are common in cohesive environments (Knight et al., 2009; Lovelock et al., 2010; Vo-Luong and Massel, 2008), it is difficult to isolate how much of the profile shape is caused by processes that occur only in the intertidal. One exception is the stabilization effect of some vegetation (e.g. mangroves and saltmarsh), which can only grow in the intertidal due to physiological restrictions. Bryan et al. (2017) explained that mangrove vegetation initially increases the currents and flood dominance just landward of the fringe of mangroves (due to tidal wave shoaling), transporting the sediment into forests. Once the sediment enters the forest, the stabilization effect of mangroves on intertidal flats can occur in both direct and indirect ways. For instance, dense vegetation attenuates these currents (Bryan et al., 2017) while mangrove roots are believed to increase the consolidation processes by dewatering of sediments that in turn stabilizes the sediments against erosion (Roskoden et al., 2019). Consequently, both effects will cause gradual accretion just inshore of the fringe. The accumulation, over time, results in the increase in slope seaward of mangroves and flatten the slope inside the mangroves, resulting in flat-topped profiles characteristic of mangrove dominated mangrove sites (Bryan et al., (2017) summarise a range of examples from other studies). The effect of our stabilization on profile development is similar. Although note that the stabilizing effect of vegetation included in conventional Delft3D models (and in Bryan et al., 2017) is only a hydrodynamic one, caused by increased drag and reduced currents, which may not be the most important way that the vegetation acts on profile evolution.

Low-tide rainfall can have substantial effects on the erodibility of surficial sediments on intertidal flats (Pilditch et al., 2008; Tolhurst et al., 2006b). Our study excluded the effect of rainfall and consequent changes to water content and direct impacts on sediment surfaces. Such an effect could easily be incorporated into our model in a future version. As discussed earlier, the stabilizing effect of exposure and vegetation on intertidal mudflats are somewhat similar and the resulting accretion patterns would tend to result in flat-topped profiles. However, the stabilization effect of exposure only happens if it does not rain, whereas mangrove stabilization occurs perpetually. The temperature and duration are essentially a proxy for water content in the sediment, and ideally water content should be directly modelled. It would be possible to incorporate rain in a water content model, or to use a time series of water content loss rate as an input file. In addition, the effect of consolidation on bed level change is not included in this research. Zhou et al. (2016) introduced a self-weight consolidation model that incorporated influences of consolidation in simulations by gradually reducing the bed level and decreasing the bed erodibility (i.e., increasing the critical bed shear stress), which led to long-term morphodynamic effects on the intertidal mudflat.

Our model was developed to predict the effect of air temperature and exposure on the evolution of bed profile based on experimental results on sediments collected from the intertidal mudflat in the Firth of Thames. The samples have specific properties characterized by the grainsize, the inundated water content, the *Chl-a* content

(as a proxy of biofilm biomass) and the organic content that will all play a role in controlling the erosional behavior of sediments, ultimately making the empirical fitting coefficients site-specific. Water content reduction and biofilm growth are believed to increase the erosion resistance (Amos et al., 2004; Black et al., 2002; Chen et al., 2017; Nguyen et al., 2019; Nguyen et al., 2020; Van Ledden et al., 2004). Nevertheless, the interaction between factors is complicated, for example, the reduction of water content might slow down the biofilm growth (Nguyen et al., 2020), meanwhile, a high *Chl-a* content on sediment surfaces might prevent evaporation (Lianfang et al., 2009; Vandevivere and Baveye, 1992).

The stabilizing effect of biofilms is often balanced by the destabilizing effect of bioturbators such as infaunal shellfish and worms (that in turn feed on the biofilms). As with biofilms, bioturbator activity is also mediated by environmental conditions. For example, Cozzoli et al. (2021) introduced a model that predicted the effect of seasonal changes in temperature on the activity of bioturbators, and their ultimate effect on sediment resuspension. The model used a mix of empirical parametrization and general theory on size and temperature scaling of metabolic rates. Zhou et al. (2022) studied the effect of heat waves on macroinvertebrates bioturbating behavior in intertidal areas, showing that the migratory behavior of bioturbating cockles increased under heat stress, thereby altering the deposition-erosion balance on tidal flats.

We did not transitioned the change in stabilization smoothly into the subtidal in our simple model development, and indeed, some of our formulations (e.g. low- *Chl-a*) caused an increase in stabilization seaward. More work is needed to parameterize these transitions realistically. In addition, one would expect exposed erosion resistance should recover to inundated conditions after submergence as water content is replenished within the sediments (Tolhurst et al., 2006a). In contrast, Nguyen et al., (2020) showed no significant change to erodibility of re-submerged and exposed sediments, which was explained by combining the effect of long- term exposure and biofilm growth. In this research, we included coefficients of recovery that allow erosion resistance decrease during immersion (increases *ER* and decreases T_{cr}). However, we do not have experimental results to inform the selection of coefficients for the recovery rate of sediments. Nevertheless, including the processes gives an indication of the importance of this term as air temperature and exposure time varied. Generally, all our models are entirely parameterized with the empirical data, and additional work is needed to generalize the model to other sites. Although our models are site-specific, the results are generally applicable to cohesive intertidal settings.

Conclusions

This study examined how exposure changes intertidal profile evolution over a short (annual) time scale (a morphological scale factor of 10 was used to shorten running time of models). The stabilizing effect of exposure is likely to be, to some extent, similar to vegetation on intertidal flats on the evolution of tidal profile, although the mechanism for causing sediment dewatering is different. Our results imply that muddy, highly stabilized

intertidal areas evolve toward flat-topped (convex) profiles more quickly when stabilization is included in the evolution.

Our models also investigated the influence of different factors such as air temperature, *Chl-a* content, bed sediment composition and spring-neap tides on the changes of bed level, all of which contribute to stabilization in different ways. Although, some of the assumptions in our models are inevitably made (the lack of precipitation, the constant exposure temperatures), the key message is consistent. Subtle differences in exposure control the convexity of the profile that evolves, and so the way in which new coastal land will build in the future to protect the coast. Ultimately, these model experiments highlight the complexities that might play a role in shaping our coast with predicted changes to storm-surge climates (which change our inundation regimes) accompanied by rising temperatures.

Acknowledgments

The University of Waikato Doctoral Scholarship for international students supported to Hieu M. Nguyen. The Tipping Points project in the Dynamic Seas programme of the New Zealand Sustainable Seas National Science Challenge (CO1x1515 4.2.1) funded Karin Bryan and Conrad Pilditch. Zeng Zhou is supported by the National Natural Science Foundation of China (Grants No. 41976156 and 51620105005), and the Natural Science Foundation of Jiangsu Province (Grants No. BK20200077).

References

Amos, C., Bergamasco, A., Umgiesser, G., Cappucci, S., Cloutier, D., DeNat, L., Flindt, M., Bonardi, M. and Cristante, S., 2004. The stability of tidal flats in Venice Lagoon—the results of in-situ measurements using two benthic, annular flumes. Journal of Marine Systems, 51(1-4): 211-241.

Bearman, J.A., Friedrichs, C.T., Jaffe, B.E. and Foxgrover, A.C.J.J.o.C.R., 2010. Spatial trends in tidal flat shape and associated environmental parameters in South San Francisco Bay. 26(2 (262)): 342-349.

Black, K., Tolhurst, T., Paterson, D. and Hagerthey, S., 2002. Working with natural cohesive sediments. Journal of Hydraulic Engineering, 128(1): 2-8.

Bryan, K.R., Nardin, W., Mullarney, J.C. and Fagherazzi, S.J.C.S.R., 2017. The role of cross-shore tidal dynamics in controlling intertidal sediment exchange in mangroves in Cù Lao Dung, Vietnam. 147: 128-143.

Chen, X., Zhang, C., Zhou, Z., Gong, Z., Zhou, J., Tao, J., Paterson, D. and Feng, Q.J.J.o.G.R.B., 2017. Stabilizing effects of bacterial biofilms: EPS penetration and redistribution of bed stability down the sediment profile. 122(12): 3113-3125.

Cozzoli, F., Shokri, M., da Conceição, T. G., Herman, P. M., Hu, Z., Soissons, L. M., ... & Bouma, T. J. (2021). Modelling spatial and temporal patterns in bioturbator effects on sediment resuspension: A biophysical metabolic approach. Science of the Total Environment, 792, 148215.

Dyer, K.J.G.S., London, Special Publications, 1998. The typology of intertidal mudflats. 139(1): 11-24.

Fagherazzi, S., Carniello, L., D'Alpaos, L. and Defina, A.J.P.o.t.N.A.o.S., 2006. Critical bifurcation of shallow microtidal landforms in tidal flats and salt marshes. 103(22): 8337-8341.

Fagherazzi, S., Viggato, T., Vieillard, A., Mariotti, G. and Fulweiler, R., 2017. The effect of evaporation on the erodibility of mudflats in a mesotidal estuary. Estuarine, Coastal and Shelf Science, 194: 118-127.

Friedrichs, C., 2011. Tidal flat morphodynamics:asynthesis. In: Eric Wolanski, E., McLusky, D.(Eds.), Treatise on Estuarine and Coastal Science, vol.3.Academic Press, Waltham: 37–170.

Friedrichs, C., Aubrey, D.J.M.i.e. and seas, C., 1996. Equilibrium Hyposometry of Intertidal. 50: 405-429.

Kirby, R.J.C.S.R., 2000. Practical implications of tidal flat shape. 20(10-11): 1061-1077.

Kirwan, M.L., Temmerman, S., Skeehan, E.E., Guntenspergen, G.R. and Fagherazzi, S.J.N.C.C., 2016. Overestimation of marsh vulnerability to sea level rise. Nature Climate Change, 6(3): 253-260.

Knight, J.M., Dale, P.E., Spencer, J., Griffin, L.J.E., Coastal and Science, S., 2009. Exploring LiDAR data for mapping the micro-topography and tidal hydro-dynamics of mangrove systems: An example from southeast Queensland, Australia. 85(4): 593-600.

Le Hir, P., Roberts, W., Cazaillet, O., Christie, M., Bassoullet, P. and Bacher, C.J.C.s.r., 2000. Characterization of intertidal flat hydrodynamics. 20(12-13): 1433-1459.

Lianfang, Z., Wei, Z. and Wei, T., 2009. Clogging processes caused by biofilm growth and organic particle accumulation in lab-scale vertical flow constructed wetlands. Journal of Environmental Sciences, 21(6): 750-757.

Liu, X.J., Gao, S. and Wang, Y.P.J.C.S.R., 2011. Modeling profile shape evolution for accreting tidal flats composed of mud and sand: A case study of the central Jiangsu coast, China. 31(16): 1750-1760.

Lovelock, C.E., Sorrell, B.K., Hancock, N., Hua, Q. and Swales, A.J.E., 2010. Mangrove forest and soil development on a rapidly accreting shore in New Zealand. 13(3): 437-451.

Mangan, S., Bryan, K.R., Thrush, S.F., Gladstone-Gallagher, R.V., Lohrer, A.M. and Pilditch, C.A.J.M.E.P.S., 2020. Shady business: the darkening of estuaries constrains benthic ecosystem function. 647: 33-48.

Marani, M., D'Alpaos, A., Lanzoni, S., Carniello, L. and Rinaldo, A.J.G.R.L., 2007. Biologically-controlled multiple equilibria of tidal landforms and the fate of the Venice lagoon. 34(11).

Mariotti, G. and Fagherazzi, S.J.J.o.G.R.E.S., 2010. A numerical model for the coupled long-term evolution of salt marshes and tidal flats. 115(F1).

Mehta, A.J., 2002. Mudshore dynamics and controls. In: Healy, T., Wang, Y., and Healy, J.A. (eds.), Muddy Coasts of the World: Processes, Deposits and Function: 19–60.

Mi, H., Fichot, C.G., Bryan, K.R., Qiao, G., Fagherazzi, S.J.E.S.P. and Landforms, 2020. Rapid shoreline flooding enhances water turbidity by sediment resuspension: An example in a large Tibetan lake. 45(15): 3780-3790.

Nguyen, H.M., Bryan, K.R., Pilditch, C.A. and Moon, V.G., 2019. Influence of ambient temperature on erosion properties of exposed cohesive sediment from an intertidal mudflat. Geo-Marine Letters: 1-11.

Nguyen, H.M., Bryan, K.R., Pilditch, C.A.J.E.S.P. and Landforms, 2020. The effect of long-term aerial exposure on intertidal mudflat erodibility. 45(14): 3623-3638.

Partheniades, E.J.J.o.t.H.D., 1965. Erosion and deposition of cohesive soils. 91(1): 105-139.

Paterson, D.M., 1989. Short-term changes in the erodibility of intertidal cohesive sediments related to the migratory behavior of epipelic diatoms. Limnology and Oceanography, 34(1): 223-234.

Pilditch, C.A., Widdows, J., Kuhn, N., Pope, N. and Brinsley, M., 2008. Effects of low tide rainfall on the erodibility of intertidal cohesive sediments. Continental Shelf Research, 28(14): 1854-1865.

Pratt, D. R., Lohrer, A. M., Pilditch, C. A., & Thrush, S. F. (2014). Changes in ecosystem function across sedimentary gradients in estuaries. Ecosystems, 17(1), 182-194.

Pritchard, D., Hogg, A.J. and Roberts, W.J.C.S.R., 2002. Morphological modelling of intertidal mudflats: the role of cross-shore tidal currents. 22(11-13): 1887-1895.

Pritchard, D. and Hogg, A.J.J.J.o.G.R.O., 2003. Cross-shore sediment transport and the equilibrium morphology of mudflats under tidal currents. 108(C10).

Roberts, W., Le Hir, P. and Whitehouse, R.J.C.S.R., 2000. Investigation using simple mathematical models of the effect of tidal currents and waves on the profile shape of intertidal mudflats. 20(10-11): 1079-1097.

Roskoden, R.R., Bryan, K.R., Schreiber, I. and Kopf, A.J.G.-M.L., 2019. Rapid transition of sediment consolidation across an expanding mangrove fringe in the Firth of Thames New Zealand. 1-14.

Tolhurst, T., Defew, E., Perkins, R., Sharples, A. and Paterson, D., 2006a. The effects of tidally-driven temporal variation on measuring intertidal cohesive sediment erosion threshold. Aquatic Ecology, 40(4): 521-531.

Tolhurst, T., Friend, P., Watts, C., Wakefield, R., Black, K. and Paterson, D.J.A.E., 2006b. The effects of rain on the erosion threshold of intertidal cohesive sediments. 40(4): 533-541.

Underwood, G.J. and Paterson, D.M., 2003. The importance of extracellular carbohydrate productionby marine epipelic diatoms. Advances in botanical research, 40: 183-240.

Van Ledden, M., Van Kesteren, W. and Winterwerp, J., 2004. A conceptual framework for the erosion behaviour of sand–mud mixtures. Continental Shelf Research, 24(1): 1-11.

van Maanen, B., Coco, G., Bryan, K.R. and Friedrichs, C.T.J.O.D., 2013. Modeling the morphodynamic response of tidal embayments to sea-level rise. 63(11-12): 1249-1262.

Van Rijn, L.C.J.A., The Netherlands, 1998. Principles of Coastal Morphology Aqua Publications.

Vandevivere, P. and Baveye, P., 1992. Effect of bacterial extracellular polymers on the saturated hydraulic conductivity of sand columns. Appl. Environ. Microbiol., 58(5): 1690-1698.

Vo-Luong, P. and Massel, S.J.J.o.M.S., 2008. Energy dissipation in non-uniform mangrove forests of arbitrary depth. 74(1-2): 603-622.

Widdows, J., Brinsley, M., Bowley, N. and Barrett, C., 1998. A benthic annular flume forin situmeasurement of suspension feeding/biodeposition rates and erosion potential of intertidal cohesive sediments. Estuarine, Coastal and Shelf Science, 46(1): 27-38.

Winterwerp, J., 2007. On the sedimentation rate of cohesive sediment, Proceedings in Marine Science. Elsevier, pp. 209-226.

Yang, S., Li, H., Ysebaert, T., Bouma, T., Zhang, W., Wang, Y., Li, P., Li, M., Ding, P.J.E., Coastal and Science, S., 2008. Spatial and temporal variations in sediment grain size in tidal wetlands, Yangtze Delta: On the role of physical and biotic controls. 77(4): 657-671.

Zhou, Z., Coco, G., van der Wegen, M., Gong, Z., Zhang, C. and Townend, I., 2015. Modeling sorting dynamics of cohesive and non-cohesive sediments on intertidal flats under the effect of tides and wind waves. Continental Shelf Research, 104: 76-91.

Zhou, Z., Ye, Q. and Coco, G.J.A.i.W.R., 2016. A one-dimensional biomorphodynamic model of tidal flats: sediment sorting, marsh distribution, and carbon accumulation under sea level rise. 93: 288-302.

Zhou, Z., Bouma, T. J., Fivash, G. S., Ysebaert, T., van IJzerloo, L., van Dalen, J., ... & Walles, B. (2022). Thermal stress affects bioturbators' burrowing behavior: A mesocosm experiment on common cockles (Cerastoderma edule). Science of the Total Environment, 824, 153621.